Supplementary Legends

Video 1 Development of ISVs in WT zebrafish embryos between 20 and 44 hpf. Time-lapse microscopy images of the developing vasculature of the trunk region of WT *Tg(fli1a:EGFP)*^{y1} embryos visualised by eGFP fluorescence. Frames were taken at 10 min intervals between 20 and 44 hpf. Shown are lateral views with the anterior to the left and the dorsal side up.

Video 2 Development of ISVs in NOSTRIN KD zebrafish embryos between 20 and 44 hpf. Time-lapse microscopy images of the developing vasculature of the trunk region of NOSTRIN KD *Tg(fli1a:EGFP)*^{y1} embryos injected with ATG MO. The vasculature was visualised by eGFP fluorescence. Frames were taken at 10 min intervals between 20 and 44 hpf. Shown are lateral views with the anterior to the left and the dorsal side up.

Supplementary Information Figure S1 Kovacevic

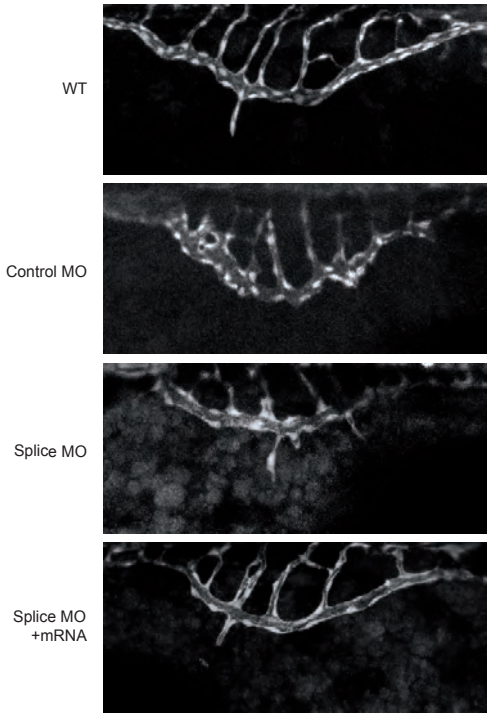

Supplementary Figure 1. Knockdown of NOSTRIN in zebrafish interferes with the development of the subintestinal vein (SIV) basket. *Tg(fli1a:EGFP)*^{y1} zebrafish embryos were injected with 3.3 ng Control MO or 5 ng Splice MO or left uninjected (WT). For the rescue 15 pg of zebrafish NOSTRIN mRNA was coinjected with Splice MO. SIV baskets were imaged at 48 hpf using CLSM. Images are lateral views with the anterior to the left and the dorsal side up.

Supplementary Information Figure S2 Kovacevic

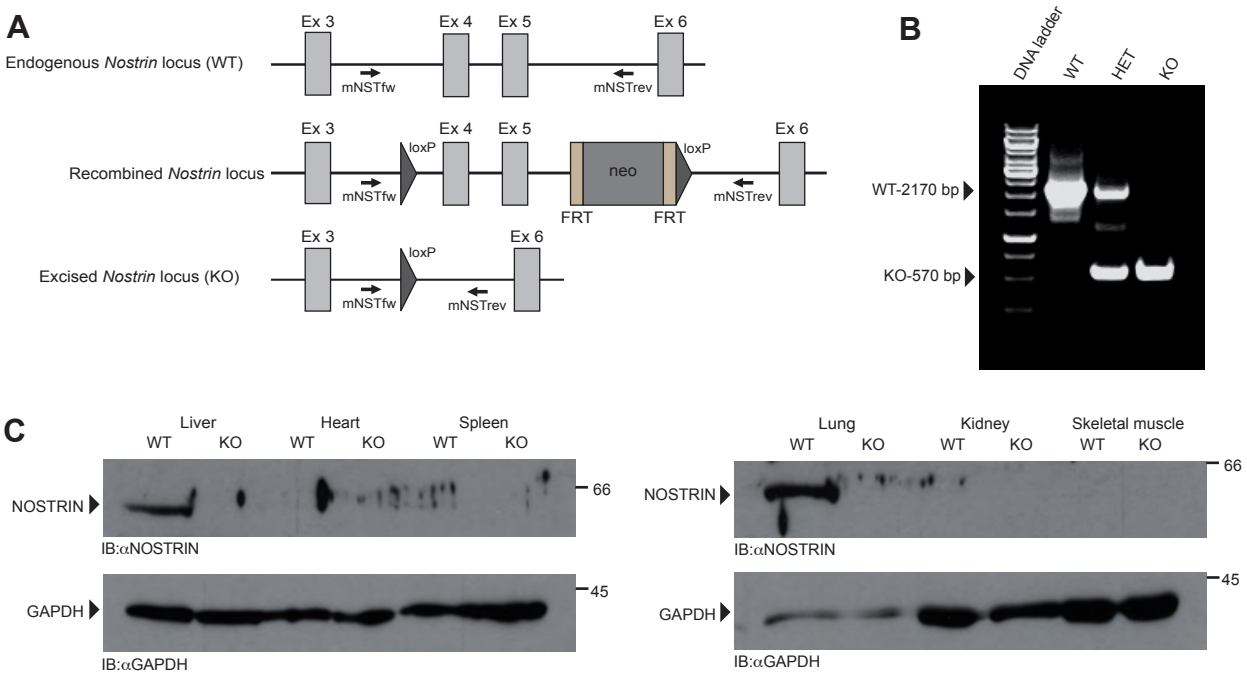

Supplementary Figure 2. (A) NOSTRIN knockout in mice is achieved by Cre-mediated excision of exons 4 and 5 of the *Nostrin* gene. Schematic presentation of the endogenous *Nostrin* locus (WT) with the binding sites for genotyping primers indicated by arrows (top). Two loxP sites and a neomycin resistance gene cassette were introduced by homologous recombination to generate the recombined *Nostrin* locus (middle). Cre-mediated excision of the loxP-flanked sequence results in deletion of the exons 4 and 5 in the *Nostrin* KO locus (bottom). (B) Genotyping of NOSTRIN KO mice by PCR. Mice were genotyped by PCR using the primers mNSTfwd (5'-CCTAGAGCTGACTCCTGCTGTGAGAGG-3') and mNSTrev (5'-CTCATACTGGTAAGCA GAAAAGCATCGTTT-3') indicated in (A). Amplified DNA sequences had the expected sizes of 2170 bp indicating the WT allel or 570 bp indicating the KO allel, respectively. (C) NOSTRIN is highly expressed in lung and liver and expression is lost in the NOSTRIN KO. Comparison of the level of NOSTRIN protein in various tissues of WT and NOSTRIN KO mice, analysed by immunoblotting with a NOSTRIN-specific polyclonal antiserum. Immunoblot against GAPDH (Abcam) is shown as loading control.

Supplementary Information Figure S3 Kovacevic

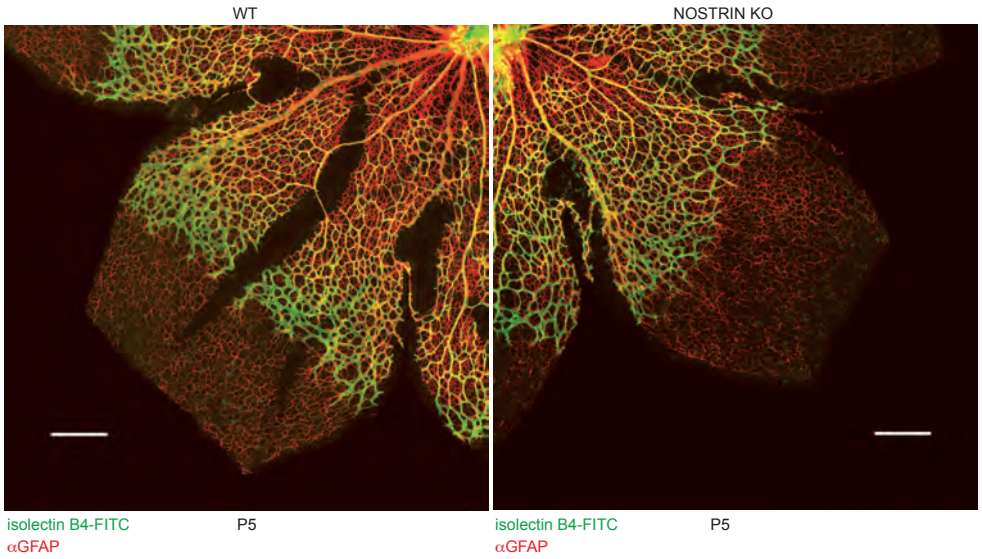

Supplementary Figure 3. Analysis of mouse retina astrocyte network. The vascular radius is greater in the retinas of WT than in the retinas of KO mice, but the radius of the astrocyte network is unchanged in the NOSTRIN KO compared to WT. Specimen were treated as described for analysis of mouse postnatal retinal angiogenesis and in addition stained with GFAP (glial fibrillary acidic protein)-specific antibody (1:1000, Dako) in combination with an Alexa 546-conjugated anti-rabbit antibody (1:200, Invitrogen). Scale bars represent 300 μm.

Supplementary Information Figure S4 Kovacevic

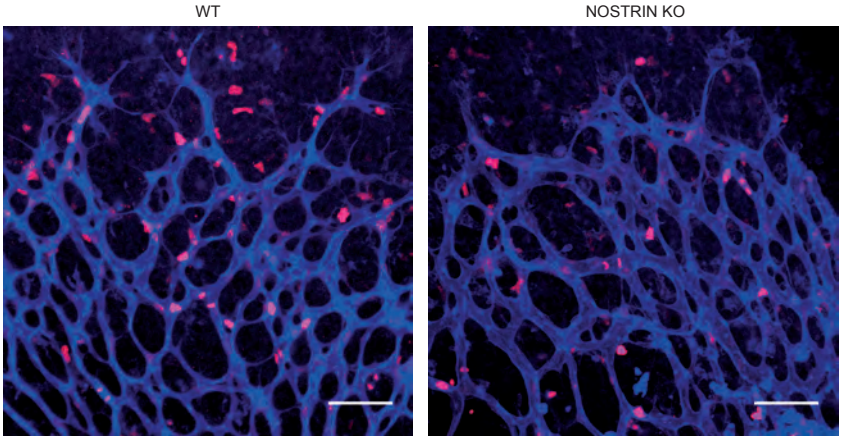

Supplementary Figure 4. Analysis of endothelial cell proliferation in mouse retina. Proliferation of endothelial cells in retinas isolated from NOSTRIN KO is decreased when compared to WT mice. Retinas were isolated from P5 WT and NOSTRIN KO mice and stained with isolectin B4-FITC and Ki67 (1:100, Millipore) in combination with an Alexa 546-conjugated anti-rabbit antibody (1:200, Invitrogen). Scale bars represent 70 µm.

Supplementary Information Figure S5 Kovacevic

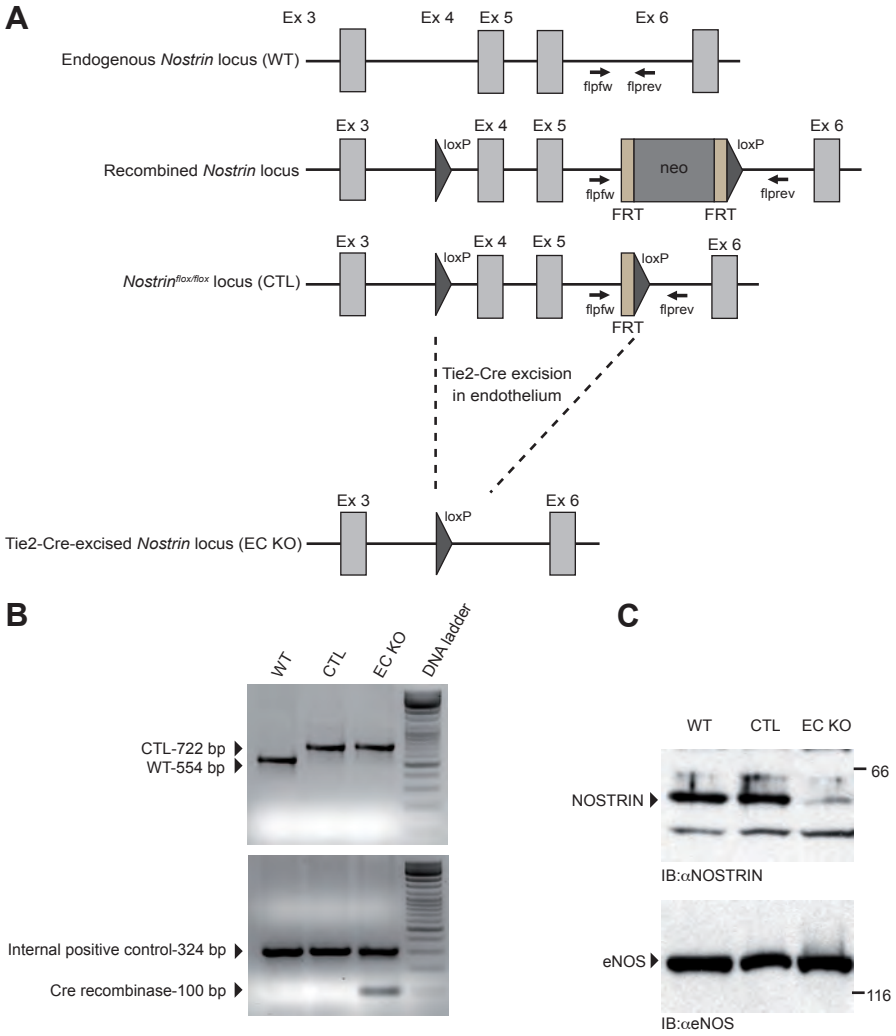

Supplementary Figure 5. (A) NOSTRIN endothelial specific knockout in mice is achieved by Cre-mediated excision of exons 4 and 5 of the *Nostrin* gene in endothelium. Schematic presentation of the endogenous *Nostrin* locus (WT) with the binding sites for genotyping primers indicated by arrows (top). Two loxP sites and a neomycin resistance gene cassette were introduced by homologous recombination to generate the recombined *Nostrin* locus (middle). Neomycin cassette was excised by crossing with Flp-recombinase-expressing deleter mice to generate *Nostrin*$^{flox/flox}$ control mice (CTL). CTL mice were further bred with Tie2-Cre mice in order to achieve the excision of the loxP-flanked sequence leading to deletion of the exons 4 and 5 in the *Nostrin* KO locus in endothelium (EC KO, bottom). (B) Genotyping of EC KO mice by PCR. EC KO mice were genotyped by PCR using the following primers: flpfw (5'-AGGTTTA TAGGAGAGCCAGGGACCTAGC-3'), flprev (5'-CTCATACTGGTAAGCAGAAAAGCATCGT TT-3'), Crefw (5'-GCGGTCTGGCAGTAAAAACTATC-3'), Crerev (5'-GTGAAACAGCATTGCTGTGACTT-3'), controlfw (5'-CTAGGCCAC AGAATTGAAAGATCT-3') and controlrev (5'-GTAGGTGGAAAT TCTAGCATCATCC-3'). Amplified DNA sequences had the expected sizes of 722 bp indicating the *Nostrin*$^{flox/flox}$ allele, the 554 bp indicating the *Nostrin* WT allele, 324 bp indicating internal positive control and 100-bp indicating Cre-recombinase. (C) The expression of NOSTRIN in lung tissue is almost completely lost in the EC KO mice. Comparison of the level of NOSTRIN protein expression in lung tissue of WT, CTL and EC KO mice, analysed by immunoblotting with a NOSTRIN-specific polyclonal antiserum. Immunoblot against eNOS (Transduction laboratories) is shown as loading control.

Supplementary Information Figure S6 Kovacevic

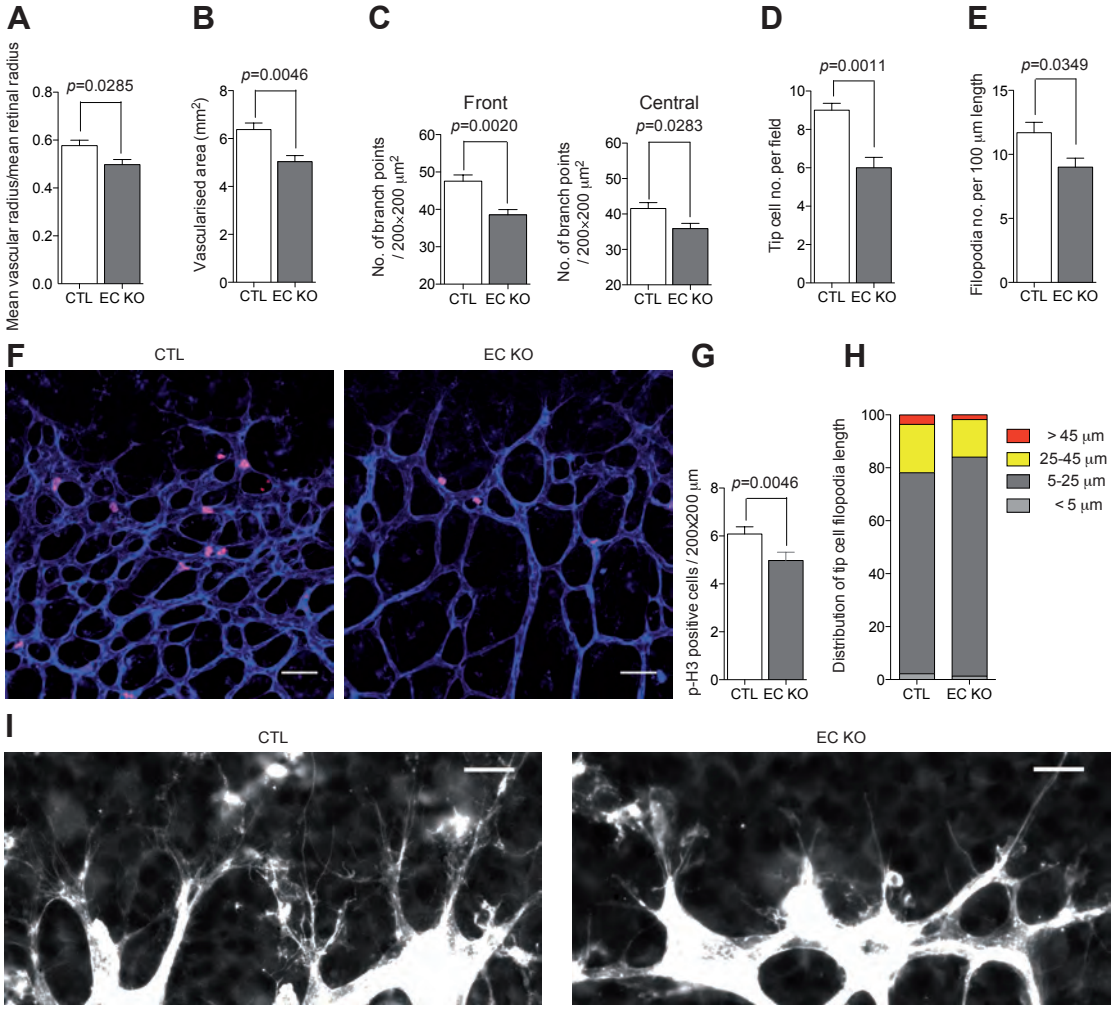

Supplementary Figure 6. Analysis of postnatal retina in NOSTRIN endothelial cell-specific KO mice (EC KO). The analysis was performed on retinas isolated from littermates *Nostrin*$^{flox/flox}$ (CTL) and *Nostrin*$^{flox/flox}$*Tie2-Cre*$^{+}$ (EC KO) at P4 as described in Materials and Methods and in Figure 3 legend. Mean vascular radius (A) and vascularised area (B) are significantly reduced in EC KO mice. The number of branch points at the vascular front (C, left) and in the central (C, right) region of the retina are reduced when compared to retinas isolated from CTL mice. In addition, the tip cell number (D) and filopodia number (E) are significantly decreased in EC KO. Furthermore, we found less proliferating cells (shown by phospho-Histone H3 staining) in EC KO retinas (overview F, quantification G). Scale bars represent 50 µm. Finally, the tip cells in retinas of EC KO mice exhibit less of long filopodia when compared to CTL mice (overview I, quantification H). Scale bars represent 20 µm. In general, the effect of endothelial cell-specific NOSTRIN KO on postnatal retinal angiogenesis in EC KO mice reproduces the effect of loss of NOSTRIN in the global NOSTRIN KO mice (Figure 3).

Supplementary Information Figure S7 Kovacevic

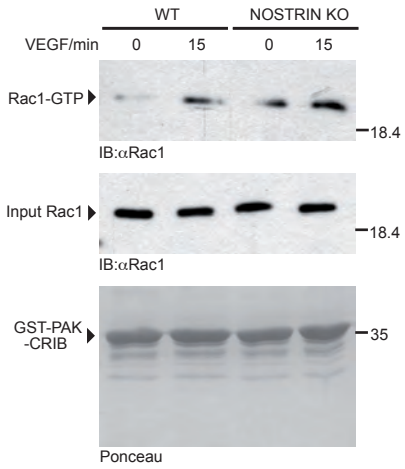

Supplementary Figure 7. Comparison of VEGF dependent activation of Rac1 in MLECs isolated from WT or NOSTRIN KO mice measured with PAK-CRIB assay. Equal amounts of Rac1 (input Rac1) and GST-PAK-CRIB were applied. The cells were starved for 6 hr and stimulated with 100 ng/ml VEGF-C (ReliaTech) as described (Wang et al. 2010). VEGF stimulation induced Rac1 activity in both WT and KO MLECs.